

Article

Green Synthesis and Characterization of Palladium Nanoparticles by Pulsed Laser Ablation and Their Antibacterial Activity

Susan H. Salman, Khawla S. Khashan *  and Aseel A. Hadi 

Department of Applied Sciences, University of Technology, Baghdad 10066, Iraq

* Correspondence: khawla.s.khashan@uotechnology.edu.iq; Tel.: +964-7713400343

Abstract: In this study, the technique of pulsed laser ablation in liquid PLAL media was successfully used to synthesize Palladium structures in nanoscale for antibacterial activity. The synthesized palladium nanoparticles (Pd NPs) were confirmed using Fourier-transform infrared spectroscopy (FT-IR), X-ray diffraction (XRD), Transmission electron microscopy (TEM), and UV-Visible spectroscopy analysis. The crystalline nature of Pd NPs with face-centered cubic structure is revealed by XRD analysis. The TEM images clearly demonstrated the spherical shape, with average particle sizes ranging from a few nanometers to several tens of nanometers. UV-vis absorption spectroscopy revealed that the absorbance intensity of the prepared Pd NPs increased as the laser fluences increased. Palladium nanoparticles were tested for antibacterial activity against two bacterial strains: Gram-negative (*Escherichia coli*) and Gram-positive (*Staphylococcus aureus*). The agar well diffusion method results revealed that Pd NPs prepared at 10.2 J/m² had a higher antibacterial activity for both bacterial strains due to the higher concentration. Furthermore, the effect of Pd NPs was stronger against Gram-negative bacteria than Gram-positive.

Keywords: palladium nanoparticles; antibacterial; pulsed laser ablation in liquid PLAL; green synthesis; noble metal nanoparticles; *Staphylococcus aureus*; *Escherichia coli*



Citation: Salman, S.H.; Khashan, K.S.; Hadi, A.A. Green Synthesis and Characterization of Palladium Nanoparticles by Pulsed Laser Ablation and Their Antibacterial Activity. *Metals* **2023**, *13*, 273. <https://doi.org/10.3390/met13020273>

Academic Editors: Jan Vrestal and Leonid M. Kustov

Received: 2 December 2022

Revised: 23 January 2023

Accepted: 28 January 2023

Published: 30 January 2023



Copyright: © 2023 by the authors. Licensee MDPI, Basel, Switzerland. This article is an open access article distributed under the terms and conditions of the Creative Commons Attribution (CC BY) license (<https://creativecommons.org/licenses/by/4.0/>).

1. Introduction

One of the most serious issues confronting state health systems today is the resistance of microorganisms that cause infection when exposed to a drug that would usually kill them or stop their growth, also known as antimicrobial resistance. Among all pathogens, *Escherichia coli* (*E. coli*) and *Staphylococcus aureus* are the most common (*S. aureus*). The most common strain of Gram-negative bacteria is *E. coli*. It is found in the lower intestine of warm-blooded organisms and can survive without oxygen. It is a rod-shaped bacterium that is motile but does not form spores. *E. coli* grows best at 37 °C and is found in the human gastrointestinal tract. *E. coli* strains are generally not harmful; however, some can cause dangerous food poisoning in humans. *S. aureus* is a strain of Gram-positive bacteria with diameters ranging from 0.5 to 1.5 μm and is distinguished by individual cocci that divide in more than one plane to form grape-like clusters. Furthermore, these bacteria do not form spores and are not mobile. *S. epidermidis* and *S. aureus* are the most studied *Staphylococci* strains. *S. aureus* can grow at temperatures ranging from 15 to 45 °C. In most cases, these bacteria are found in the human body's skin and nasopharynx. *S. aureus* can cause non-life-threatening skin infections, nose infections, and gastrointestinal tract infections. To diversify treatments and avoid the development of resistances as much as possible, new approaches are focusing on noble metal nanoparticles.

In general, nanotechnology science is a multidisciplinary frontier research area. One of the emerging fields in material science is the environmentally friendly synthesis of noble metal nanoparticles. The platinum group includes the transition metals Ag, Au, Pt, and Pd [1]. Among all nanoparticles, Palladium nanostructure (Pd NP) materials have recently become a new player in the sectors of nanomedicine and optoelectronics due to

their biocompatibility, adaptability to the environment, and physicochemical properties such as high thermal stability, good chemical stability, remarkable photocatalytic activity, electronic properties, and optical properties [2,3] that vary depending on size and shape, as well as their large surface area [4]. Palladium nanoparticles (Pd NPs) have recently demonstrated a significant potential for the development of antimicrobials and wound healing techniques, and antioxidant and anticancer properties [5]. There have been numerous reports demonstrating the superior properties of noble metals. However, very few studies have been conducted to investigate the benefits of Pd NPs in biomedical applications. For instance, Adams et al. [6] reported an anti-microbial effect of palladium nanoparticles on Gram-negative *Escherichia coli* and Gram-positive *Staphylococcus aureus* bacterial cultures, with a greater inhibition in the latter strain, which may be due to the stronger resistance of the cell wall of negative bacteria compared with positive bacteria. Surprisingly, the anti-bacterial activity varied depending on the NP size and time periods studied. Palladium nanoparticles' antibacterial properties were later confirmed on *E. coli* and *S. aureus* cultures [7], as well as on the novel multidrug-resistant *Cronobacter sakazakii* strain, in which NPs were able to eradicate biofilm bacterial growth, which was responsible for their multidrug resistance [8]. In this regard, this report and studies include the synthesis, characterization, and applications of antimicrobial palladium nanoparticles.

There are different methods for the synthesis of palladium nanoparticles which can be classified into chemical and physical groups. Chemical reduction typically employs reducing agents to produce nanoparticles of varying sizes and compositions; for example, Nguyen et al. [9] synthesized Pd NPs of varying sizes and shapes using the polyol method. The hydrothermal method is a simple and low-cost method for producing nanoparticles that allows the crystal structure of the resultant particles to be changed by adjusting parameters such as temperature, precursor concentration, and pressure. Chang et al. [10] used a hydrothermal method to obtain ZnO modified with varying amounts of Pd NPs. However, many of these techniques use hazardous solvents or hazardous reducing or stabilizing agents, or generate toxic pollutants and by-products [11], in addition to the nanoparticles' low uniformity and dispersivity. There are also physical methods, such as ball milling, electric arc discharge, flame pyrolysis, and laser ablation, which are used to synthesize nanoparticles [12]. Although these methods do not use toxic chemicals, they frequently require expensive instruments as well as high temperatures and pressures, which require a tremendous amount of energy [13]. As a result, various techniques for the synthesis of various nanoparticles under ambient conditions using nontoxic reagents and solvents are urgently needed [14].

Among a wide spectrum range of physical approaches, the pulsed laser ablation in liquid medium technique (PLAL) has emerged in recent years, and has been demonstrated to be a promising and efficient technique for altering the particle sizes of manufactured nanostructured materials because of the primary benefits of obtaining stable and dispersed NPs and nano-colloids, as well as the absence of contaminants. Pulsed laser ablation in liquid (PLAL) was introduced as a manufacturing technique and tested for a variety of nanoparticle compositions, including metals, semiconductors, carbon-based nanomaterials, and alloys. This technology is based on applying high-intensity pulses on a liquid material's surface. Nanoparticles are produced through near-field ablation, coulomb explosions, and photothermal ablation [15–21]. The resulting nanoparticles are then subjected to the secondary effects of laser pulses, such as liquid shock waves. Typically, cavitation bubbles are generated by LAL fragment particles separated from the bulk material. Furthermore, the particles may agglomerate repeatedly to form homogeneous nanoparticles of varying sizes [22]. The same processes might be used with several types of materials to create nanostructures in a variety of forms and sizes. As a result, this method may be described as a straightforward, efficient, and inexpensive technique for creating a variety of high-purity materials that are sought. Furthermore, as with other synthetic processes, when nanostructured materials are synthesized inside the liquid route, contaminant generation that could be harmful to the environment is avoided. This method is frequently used to

examine the impact of its effective parameters on particle sizes due to all of these factors. Laser parameters such as flux, laser wavelength, and the duration of irradiation are used to precisely control the size of particles released by the material [23–28]. Marzun et al. investigated the effect of different salts on the size of palladium nanoparticles produced by pulsed laser ablation in liquid [29]. Pd ablation in deionized water produces a bimodal size distribution with large NPs causing colloidal instability. Mendivil et al. [30] investigated the effect of ablation fluence variation on the size of Pd NPs formed in different liquids. They found that in distilled water, the average size of NPs increased as ablation fluence decreased, whereas the opposite effect was observed on the other solutions. Furthermore, palladium nanoparticles were created in an aqueous solution by Cristoforetti G. et al. [31] using an Nd:YAG pulsed laser with fluence of 21 J/cm² (with and without the addition of SDS). Kim J. et al. [32] produced homogeneous spherical palladium nanoparticles with a limited size distribution by using pulsed laser ablation on a solid Pd foil target suspended in deionized water, and they established that shorter wavelengths and lower laser fluence are more suited for producing tiny NPs. Additionally, Boutinguiza et al. [33] observed that employing a CW laser helps to better manage the nanoparticles' size distribution while manufacturing Pd NPs in comparison with pulsed Nd:YAG lasers. A few studies have been published on the production of palladium nanoparticles via laser ablation in liquid. However, no research has been conducted on the use of such Pd NPs produced in water by laser ablation as an antimicrobial against two bacterial strains. So far, no work has been done to compare two bacterial strains, Gram-positive and Gram-negative, which is the aim of this study.

The goal of this study is to use the easy and effective pulsed laser ablation in liquid (PLAL) technique to prepare nanometallic palladium (Pd) nanoparticles and assess their antibacterial activity against the various strains of tested microbes (*Streptococcus aureus*, and *Escherichia coli*).

2. Materials and Methods

2.1. Preparation of Palladium Nanoparticles (Pd NPs)

To obtain palladium nanoparticles, a palladium target (Pd, diameter of 1 cm and thickness of 3 mm, purity of 99.91%) immersed in 3 mL of Deionized water (DIW) in a small glass vessel, was ablated, using a nanosecond Q-switched Nd:YAG pulsed laser emitting radiation at wavelength 1064 nm, frequency 1 Hz, and pulse width 9 ns. The Nd:YAG laser beam was focused by an 80 mm convex lens on the upper surface of the palladium target with different laser fluences of (2.04, 4.08, 6.12, 8.16, and 10.2) J/cm² at 100 pulses. The concentration of palladium nanoparticles was prepared by weighing the target by using a four digit-balance prior to the ablation process. The target was then dried by an air dryer and weighed after ablation for each ablation process. The amount of the target mass that was ablated (ΔM) could be determined from the following equation:

$$\Delta M (\Delta g) = m_1 - m_2 \quad (1)$$

where m_1 is the target mass before ablation and m_2 is the target mass after ablation. The mass concentration was then determined by dividing the ablated mass (ΔM) by the liquid volume:

$$\text{Mass concentration } (\mu\text{g mL}^{-1}) = \Delta M / \text{liquid volume.}$$

2.2. Characterization Techniques

The functional group vibrations of the synthesized palladium nanoparticles were analyzed using Fourier-transform infrared spectroscopy FT-IR (SPECTRUM TWO N spectrometer, PerkinElmer, Yokohama, Japan) by the KBr pellet technique in the range of 400–4000 cm⁻¹. The crystalline structure of the produced Pd NPs was characterized using an X-ray diffractometer (PODWE XRD 2700AB, HAOYuan INSTRUMENT, Dandong, China). XRD analysis was recorded by Cu K α radiation with the wavelength of 1.54060 Å using a PANalytical X-PERTO PRO diffractometer system in the range from 10 to 80. The

average crystalline size was calculated from the width of the XRD peaks using Scherrer's formula $D = 0.94\lambda / \beta \cos\theta$, where β is full width at half maximum (FWHM) of the diffraction peak, λ is the wavelength of X-ray, and θ is the diffraction angle. The sample of X-ray diffraction measurement was prepared by depositing palladium nanoparticles on a silicon substrate via the drop-casting technique. Palladium nanoparticles synthesized were subjected to HR-TEM analysis using a Philips/em208 s (JEOL Ltd., Tokyo, Japan) instrument with an accelerating voltage of 200 kV and a copper micro-grid mesh (gold-coated copper grid 200 meshes) for sample preparation. The sample was prepared by depositing a drop of palladium nanoparticles onto the mesh surface, which was then left to dry at room temperature. UV-Visible spectroscopy was used to analyze the optical characteristic of the synthesized palladium nanoparticles in the wavelength range of 200 to 500 nm using a Shimadzu spectrophotometer (1900i, Shimadzu, Kyoto, Japan). These measurements were performed using a quartzite cell with a 1 cm optical path at room temperature.

2.3. Antibacterial Study of Palladium Nanoparticles

The antibacterial activity of the palladium nanoparticle suspension was examined against two types of bacteria: *Escherichia coli* (*E. coli*) and *Streptococcus aureus* (*S. aureus*).

The suspensions of bacteria were prepared by adjusting with 0.5 McFarland turbidity standard (5×10^7 cell mL⁻¹) tubes. Each type of bacteria was a subculture on nutrient broth. The stock cultures for these two bacterial isolates were placed into Mueller Hinton agar medium, cultured overnight at 37 °C, and kept in the refrigerator at 4 °C for future use. Mueller Hinton agar was used to reveal the antibacterial effectiveness. According to the producer, it was synthesized by dissolving 3.8 g of powder in 100 mL of distilled water. Then, it was dissolved via rising temperature using a heater with continuous shaking. The Mueller Hinton agar was then sterilized in an autoclave at 121 °C for 15 min, cooled in cold water at 47 °C, and resolidified in Petri dishes. These dishes were left for 15 min to cool down to room temperature.

McFarland solution was prepared utilizing BaCl₂·0.2H₂O (0.05 mL, 1.175%) and H₂SO₄ (9.95 mL, 1%). The normal solution, containing up to 5×10^7 bacterial cells per milliliter, was compared with the turbidity bacterial suspension. The two were then combined to ensure suspension. The McFarland suspension was tightly closed to avoid evaporation and wind and covered with aluminum foil to keep it away from light.

Antibacterial activity of Pd NPs against *E. coli* and *S. aureus* was measured by the well diffusion method. The bacteria were separated at the surface of the Mueller Hinton agar plates. Wells with diameters of about 6 mm were made at the surface of the agar media by the tip of a micropipette, and then Pd NP suspensions with different concentrations were added into the wells. These plates were kept in the incubator for 24 h. The inhibitory zone was repeatedly measured using a ruler and various orientations to assess the antibacterial effectiveness of the palladium nanoparticles [34].

3. Results & Discussion

Figure 1 displays the FTIR spectra of palladium nanoparticles prepared by 1064 nm Nd:YAG laser ablation of the palladium target in distilled water with different laser fluences (2.04, 6.12, and 10.2) J/cm² at 100 pulses. The intensity of the FTIR spectrum varied with laser fluence, whereas the width of the observed peaks remained relatively constant, owing to the increased amount of ablated material produced from the target surface, which causes scattering of laser light and increased absorption of solution, resulting in a decrease in the transmission spectrum. The characteristic intense peak at 3438 cm⁻¹ is due to O–H stretching of water molecules/–OH groups. The peak at 1623 cm⁻¹ is because of the H–O–H bending stretching mode. Further, the peak in the region of ~667 cm⁻¹ may be due to the presence of Pd nanoparticles [35,36].

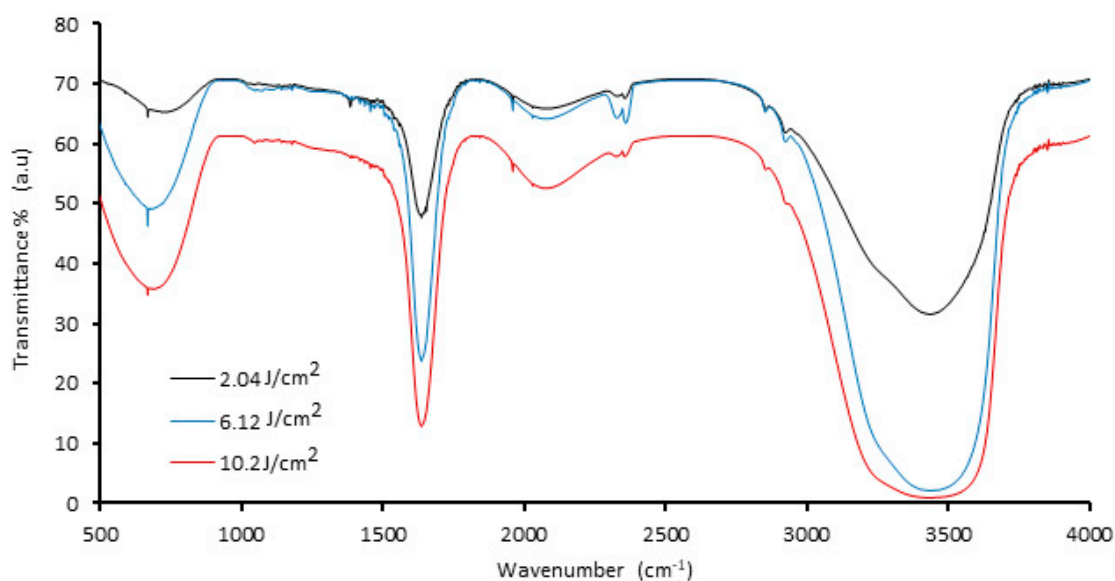


Figure 1. FTIR spectra of palladium nanoparticles (Pd NPs) synthesized via pulsed laser ablation of palladium target in distilled water with different laser fluences at 100 pulses.

The diffraction patterns of palladium nanoparticles prepared by pulsed laser ablation of the palladium target in distilled water with different laser fluences (2.04, 6.12, and 10.2) J/cm^2 for 100 pulses are shown in Figure 2. It shows that the palladium target's diffraction pattern is consistent with the typical face-centered cubic (FCC) structure of metallic palladium (JCPDS-ICDD ref.00-005-0681), with a strong reflection peak at 46.842° which, in contrast with the other reflections, may indicate the desired development track of the nanocrystals [37–40]. The elemental nature of the Pd NPs synthesized was confirmed by XRD analysis. All Pd NPs synthesized with different laser fluences are crystalline palladium with characteristic diffraction peaks (111), (200) (JCPDS card no.00-001-1201) at 2θ values of 40.585° and 46.842° , respectively, in the case of $2.04 \text{ J}/\text{cm}^2$ laser fluence (Figure 2a), whereas it was observed at 40.367° and 46.89° in the case of $6.12 \text{ J}/\text{cm}^2$ (Figure 2b); and it appeared at 40.345° and 46.842° for the laser parameter of $10.2 \text{ J}/\text{cm}^2$ (Figure 2d).

Notable peaks at diffraction angles of 34.376° and 60.808° also appeared in Figure 2a for the sample prepared at $2.04 \text{ J}/\text{cm}^2$, corresponding to (101), (200) planes (JCPDS card No. 002-1432) for the PdO phase which results from the interaction of palladium plasma plume ablation products (palladium atoms or ions) with oxygen species from water decomposition [5]. In the case of laser fluence of $6.12 \text{ J}/\text{cm}^2$, however, additional peaks centered at angles of 34.287° and 67.773° were observed, which correspond to (101), (220) planes for the PdO and Pd phases, respectively. The XRD pattern of Pd NPs prepared at $10.2 \text{ J}/\text{cm}^2$ also revealed peaks at diffraction angles of 34.259° and 60.242° , which correspond to the (101), (103) planes for PdO (JCPDS card No. 002-1432). All these peaks confirm the crystal structure of the as-prepared Pd NPs.

Table 1 contains all of the data obtained from the XRD results. The average particle size of nanoparticles increased with decreasing laser energy fluence, which is consistent with previous literature [30].

The morphology, size, and crystal structure of palladium nanoparticles prepared by pulsed laser ablation of the palladium target in distilled water were investigated using Transmission Electron Microscopy (TEM). Figures 3–5 depict TEM images of palladium nanoparticles prepared with different laser fluences of the same laser pulses (100). The TEM images revealed that laser fluences have a significant impact on particle size and the size distribution. The TEM images showed that the Pd nanoparticles in the colloidal had an almost spherical shape with a size range from few nanometers to several tens of nanometers and an average diameter of $\sim 45 \text{ nm}$ for the sample prepared with $2.04 \text{ J}/\text{cm}^2$ at 100 pulses (Figure 3). Figures 4 and 5 are TEM images and size distributions for particles

prepared with laser fluences of (6.12 and 10.2) J/cm² at a constant 100 pulses, respectively. The NPs produced were nearly spherical in shape with average diameters of 9 and 11 nm, respectively. The peaks of the size distribution of palladium nanoparticles Pd NPs prepared with various fluences (2.04, 6.12, and 10.2) J/cm² became broader with increasing laser fluence, indicating that particle size increases with increasing laser fluence [30]. It has been found that as laser fluence increases, more energy is delivered to the target, causing melting and removal of the material. Small metal droplets are fragmented by laser beam interaction, followed by rapid quenching, resulting in the formation of larger nanoparticles with a wide size distribution [41,42]. The laser fluence influences particle production rate as well. Because of the high energy, a large portion of the Pd target can be ablated at a higher laser fluence, resulting in large-scale production of Pd nanoparticles [41–43].

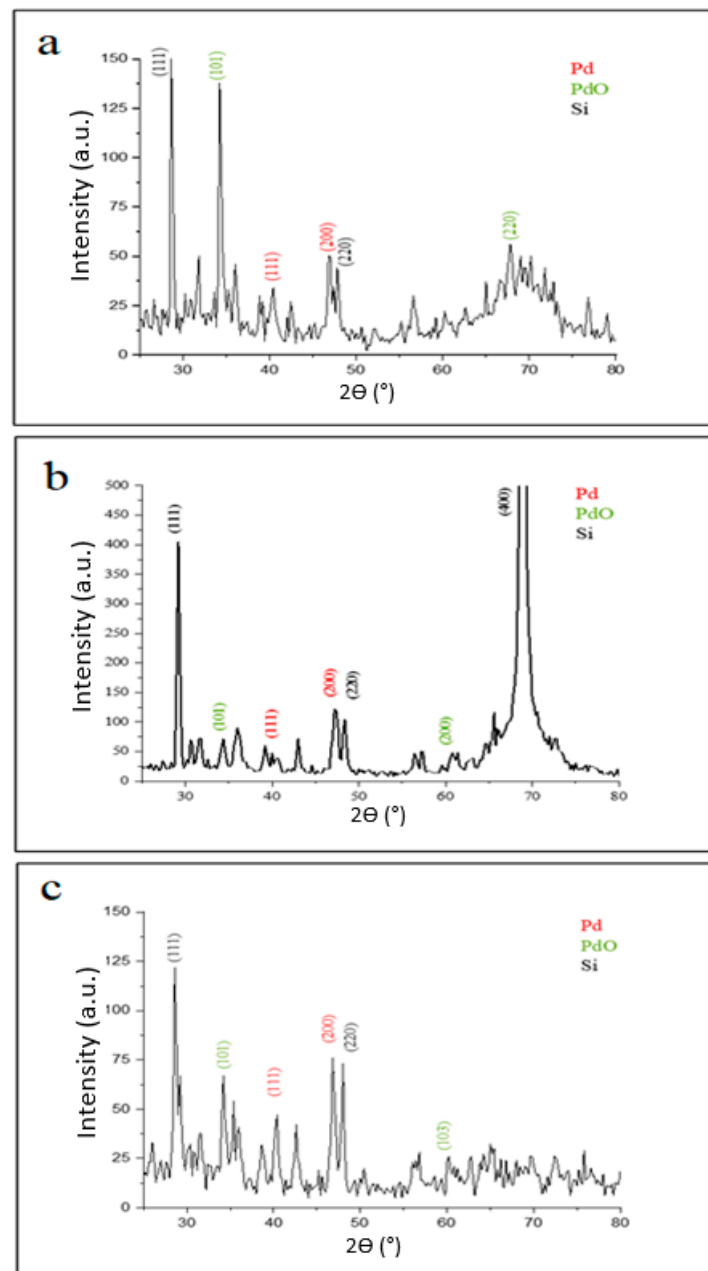
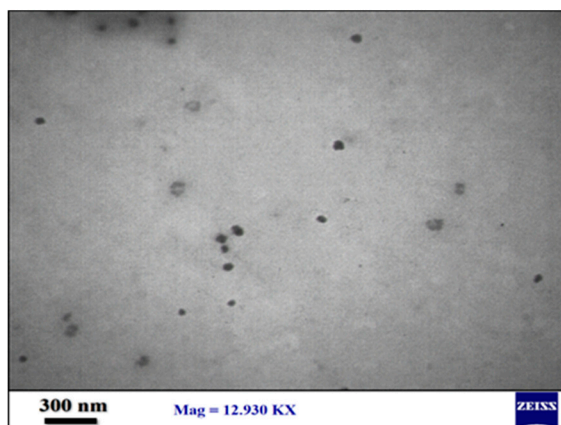


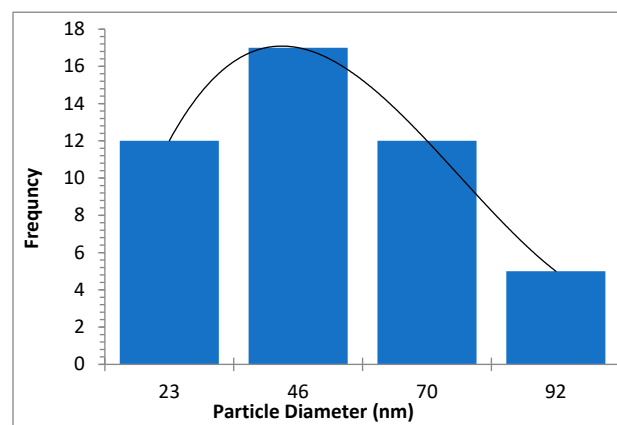
Figure 2. XRD patterns of palladium nanoparticles (Pd NPs) prepared by pulsed laser ablation of palladium target in distilled water with different laser fluences of (a) 2.04 J/cm², (b) 6.12 J/cm², and (c) 10.2 J/cm².

Table 1. The crystalline size (CS) of palladium nanoparticles (Pd NPs) prepared by 1064 nm laser ablation of palladium target in distilled water with different fluences 2.04 J/cm², 6.12 J/cm², and 10.2 J/cm² at 100 pulses.

Laser Fluence (J/cm ²)	Theta (deg)	FWHM (deg)	d _{hkl} (nm)	Orientation (hkl)	Type	CS (nm)	Av. CS (nm)
2.04	40.585	1.221	0.2221	(111)	Pd	14	12
	46.842	0.836	0.19219	(200)	Pd	10	
	34.376	0.785	0.26067	(101)	PdO	10	8.5
	60.808	1.172	0.1522	(200)	PdO	7	
6.12	40.367	0.666	0.22325	(111)	Pd	11	11
	46.89	0.663	0.1936	(200)	Pd	10	
	67.773	0.516	0.13815	(220)	Pd	12	13
	34.287	0.356	0.26132	(101)	PdO	13	
10.2	40.345	0.593	0.22337	(111)	Pd	7	8.5
	46.842	0.513	0.19379	(200)	Pd	10	
	34.259	0.448	0.26153	(101)	PdO	19	15.5
	60.242	0.72	0.1535	(103)	PdO	12	

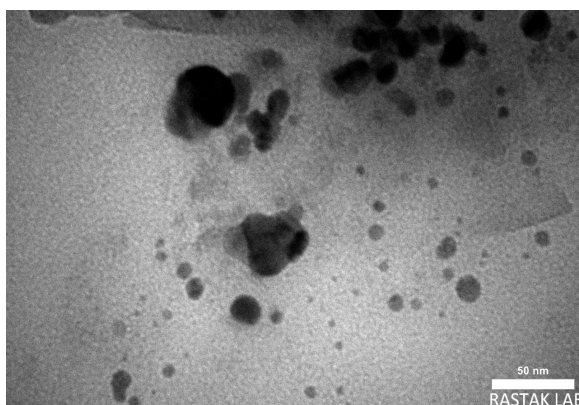


(a)

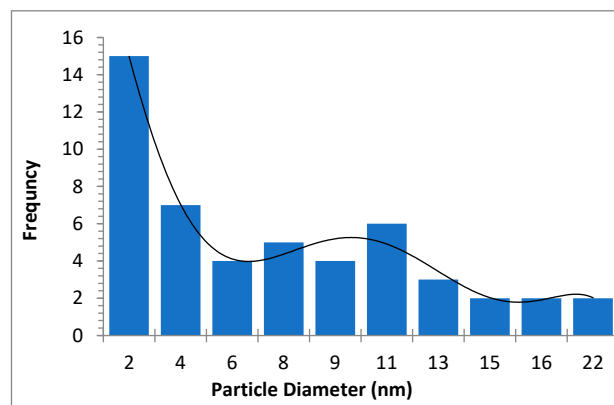


(b)

Figure 3. (a) TEM image of palladium nanoparticles (Pd NPs) prepared by pulsed laser ablation of palladium target in distilled water at 2.04 J/cm², (b) size distribution.



(a)



(b)

Figure 4. (a) TEM image of palladium nanoparticles (Pd NPs) prepared by pulsed laser ablation of palladium target in distilled water at 6.12 J/cm², (b) size distribution.

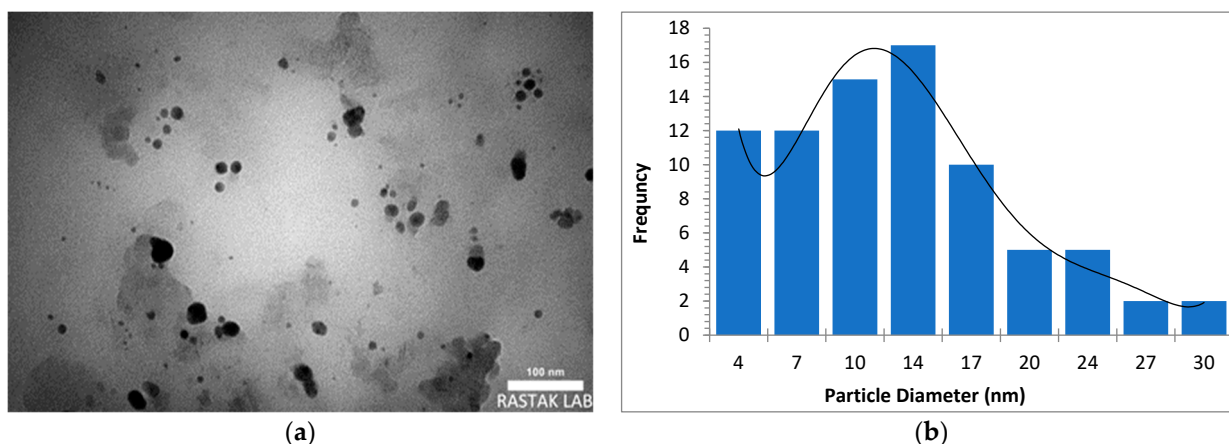


Figure 5. (a) TEM image of palladium nanoparticles (Pd NPs) prepared by pulsed laser ablation of palladium target in distilled water at 10.2 J/cm^2 , (b) size distribution.

Figure 6 illustrates the UV visible spectra of palladium nanoparticles prepared by pulsed laser ablation of a palladium target in distilled water with 100 pulses at different laser fluences. The obtained UV-vis absorption spectra show broad absorption bands, which correspond to typical inter-band transitions of metallic systems and are most likely due to ionic Pd^{2+} absorbance. The spectra clearly show that as the laser fluence increases, the absorption edge shifts towards longer wavelengths (red shift). The shift in the maximum absorption edge could be due to crystallite size increasing with laser fluence. This is supported by the TEM and size distribution diagram analyses (Figures 3–5) [39,40,43]. Furthermore, the intensity of the absorbance varies dramatically with laser fluence. The absorbance increases as laser fluences increase, which is due to an increase in the ratio of the resulting ablation, which leads to an increase in the number of particles absorbed by the delivering laser fluence and thus increases absorbance [30]. The particles synthesized at a laser fluence of 10.2 mJ/cm^2 had the highest absorbance. This is because the electronic energy levels in nanoparticles are not continuous, as they are in bulk materials. This can result in sharp and intense absorption features corresponding to nanoparticle inter-band transitions [43,44].

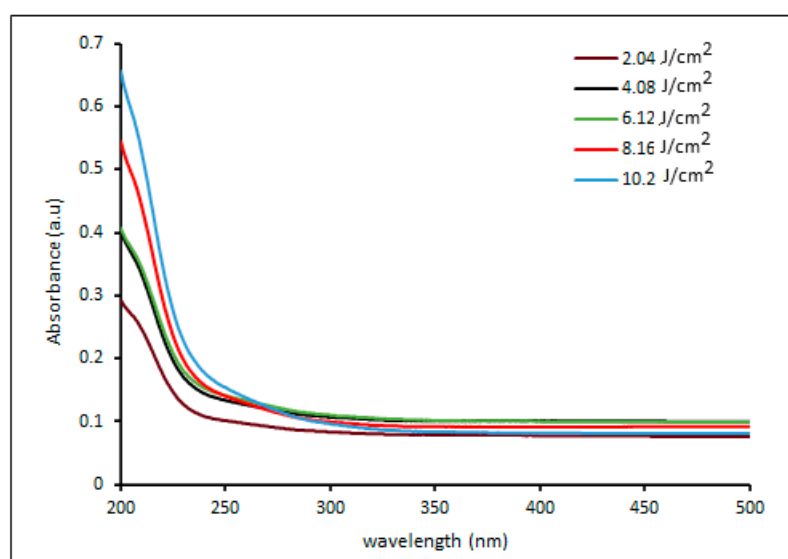


Figure 6. UV-vis absorbance spectra of palladium NPs colloidal prepared by pulsed laser ablation of palladium target in DI water with different laser fluences.

Figure 7 shows the antibacterial activity of palladium nanoparticles prepared by PLA of a palladium target in DI water with various laser fluences against both *E. coli* and *S. aureus* using the agar-well diffusion method.

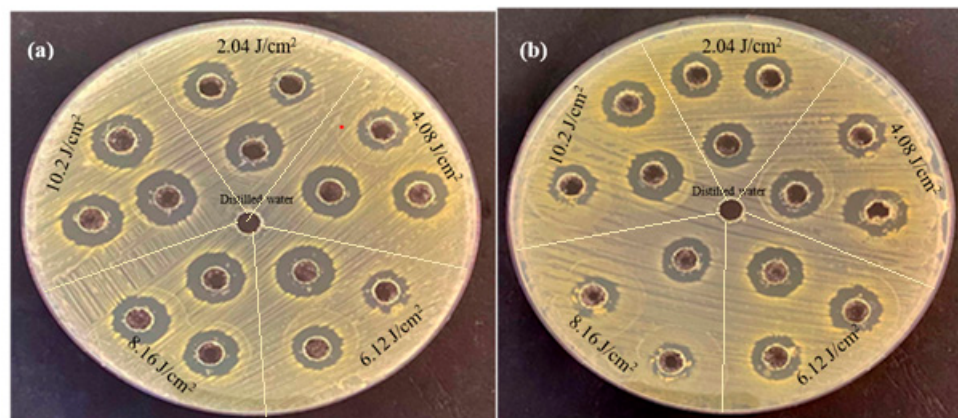


Figure 7. The antibacterial activity of palladium nanoparticles (Pd NPs) prepared by pulsed laser ablation of palladium target in DI water with different laser fluences against bacterial strains (a) *E. coli* and (b) *Staphylococcus aureus*.

It is clearly seen that at the same concentrations and conditions, the inhibition zone in *E. coli* is larger than that in *S. aureus*. The inhibition zone diameters for *E. coli* treated with palladium nanoparticles were 13.66, 15.33, 18, 18.33, and 19.66 mm, whereas for *S. aureus* they were 13, 14.66, 15.33, 15.66, and 17.66 mm (Table 2). According to these findings, *E. coli* was more sensitive to palladium nanoparticles than *S. aureus*, as reported in Table 2.

Table 2. The antibacterial activity of palladium nanoparticles (Pd NPs) prepared by pulsed laser ablation of palladium target in DI water with different laser fluences against *E. coli* and *Staphylococcus aureus* bacterial strains.

Laser Fluences (J/cm ²)	Mass Concentration (µg/mL)	Microorganisms	
		<i>E. coli</i>	<i>S. aureus</i>
Control	Control	6 ± 0	6 ± 0
2.04	200	13.66 ± 2.51	13 ± 1
4.08	300	15.33 ± 2.51	14.66 ± 3.05
6.12	400	18 ± 0.57	15.33 ± 2.51
8.16	500	18.33 ± 1.52	15.66 ± 2.08
10.2	600	19.66 ± 1.52	17.66 ± 1.52

Furthermore, the antibacterial activity of palladium nanoparticles increased as the laser fluences increased. The greater inhibitory effect at the high laser fluence of 10.2 J/cm² is due to the higher palladium nanoparticle concentration produced at this fluence. The concentration of the prepared nanoparticles increases as the laser fluence increases; this was the main reason for this effect and this corresponds to the UV-vis results. Palladium nanoparticles have a distinct antibacterial efficacy against both Gram-negative and Gram-positive bacteria, as evidenced by palladium nanoparticles' ability to inhibit the growth of *S. aureus* [37].

The laser fluence, and thus the amount of NPs, was the primary influence that affected the antibacterial effect in the current study, rather than the size of NPs. The bactericidal activity of palladium nanostructure materials includes a combination of physical and chemical impacts. Palladium nanoparticles can cause structural and morphological damage to bacterial cell membranes as a physical effect. Chemically, the interaction between

palladium nanoparticles and the bacteria's surface may result in the generation of reactive oxygen species (ROS) [45]. The latter entails the production of H₂O₂ and the release of Pd ions in an environment containing bacteria, which allows bacteria to penetrate the cell wall and exert their toxicity [46]. Palladium nanoparticles' effects on bacteria are summarized by their direct interaction, which affects the permeability of the outer membrane, has the ability to form a cavity on the surface of the bacterial cell membrane, causes intracellular oxidative stress, inhibits cell development, and eventually leads to bacterial death [45,47,48].

4. Conclusions

In this study, we investigated the successful rapid production of crystalline Pd nanoparticles by pulsed laser ablation of palladium target in DI water. Fourier-transform infrared spectroscopy (FT-IR), X-ray diffraction (XRD), Transmission electron microscopy (TEM), and UV-Visible spectroscopy were used to examine the palladium nanoparticles' properties such as composition, structure, morphology, and size distribution. The produced palladium nanoparticles (Pd NPs) are almost spherical, with face-centered cubic structure and average size in the range of few nm to several tens of nm depending on the laser fluence. Eco-friendly Pd NPs demonstrated potent antibacterial activity in all tested strains, particularly Gram-negative bacteria. Thus, this nanomaterial could be used as an alternative ingredient in antimicrobial drugs.

Author Contributions: Conceptualization, K.S.K. and A.A.H.; methodology, K.S.K.; software, S.H.S.; validation, K.S.K., A.A.H. and A.A.H.; formal analysis, S.H.S.; investigation, A.A.H.; resources, A.A.H.; data curation, S.H.S.; writing—original draft preparation, K.S.K.; writing—review and editing, K.S.K. and A.A.H.; visualization, A.A.H.; supervision, K.S.K. and A.A.H.; project administration, K.S.K.; funding acquisition, S.H.S. All authors have read and agreed to the published version of the manuscript.

Funding: This research received no external funding.

Data Availability Statement: Not applicable.

Acknowledgments: This work was supported by the Applied Science department, University of Technology—Iraq.

Conflicts of Interest: The authors declare no conflict of interest.

References

1. Anju, A.R.Y.A.; Gupta, K.; Chundawat, T.S. In vitro antimicrobial and antioxidant activity of biogenically synthesized palladium and platinum nanoparticles using *Botryococcus braunii*. *Turk. J. Pharm. Sci.* **2020**, *17*, 299.
2. Chen, A.; Ostrom, C. Palladium-based nanomaterials: Synthesis and electrochemical applications. *Chem. Rev.* **2015**, *115*, 11999–12044. [[CrossRef](#)] [[PubMed](#)]
3. Saldan, I.; Semenyuk, Y.; Marchuk, I.; Reshetnyak, O. Chemical synthesis and application of palladium nanoparticles. *J. Mater. Sci.* **2015**, *50*, 2337–2354. [[CrossRef](#)]
4. Narayanan, R.; El-Sayed, M.A. Catalysis with transition metal nanoparticles in colloidal solution: Nanoparticle shape dependence and stability. *J. Phys. Chem. B* **2005**, *109*, 12663–12676. [[CrossRef](#)] [[PubMed](#)]
5. MubarakAli, D.; Kim, H.; Venkatesh, P.S.; Kim, J.W.; Lee, S.Y. A Systemic Review on the Synthesis, Characterization, and Applications of Palladium Nanoparticles in Biomedicine. *Appl. Biochem. Biotechnol.* **2022**, 1–20. [[CrossRef](#)]
6. Adams, C.P.; Walker, K.A.; Obare, S.O.; Docherty, K.M. Size-dependent antimicrobial effects of novel palladium nanoparticles. *PLoS ONE* **2014**, *9*, e85981. [[CrossRef](#)]
7. Surendra, T.V.; Roopan, S.M.; Arasu, M.V.; Al-Dhabi, N.A.; Rayalu, G.M. RSM optimized Moringa oleifera peel extract for green synthesis of M. oleifera capped palladium nanoparticles with antibacterial and hemolytic property. *J. Photochem. Photobiol. B Biol.* **2016**, *162*, 550–557. [[CrossRef](#)] [[PubMed](#)]
8. Hazarika, M.; Borah, D.; Bora, P.; Silva, A.R.; Das, P. Biogenic synthesis of palladium nanoparticles and their applications as catalyst and antimicrobial agent. *PLoS ONE* **2017**, *12*, e0184936. [[CrossRef](#)] [[PubMed](#)]
9. Nguyen, V.L.; Nguyen, D.C.; Hirata, H.; Ohtaki, M.; Hayakawa, T.; Nogami, M. Chemical synthesis and characterization of palladium nanoparticles. *Adv. Nat. Sci. Nanosci. Nanotechnol.* **2010**, *1*, 035012. [[CrossRef](#)]
10. Chang, Y.; Xu, J.; Zhang, Y.; Ma, S.; Xin, L.; Zhu, L.; Xu, C. Optical properties and photocatalytic performances of Pd modified ZnO samples. *J. Phys. Chem. C* **2009**, *113*, 18761–18767. [[CrossRef](#)]

11. Joudeh, N.; Saragliadis, A.; Koster, G.; Mikheenko, P.; Linke, D. Synthesis methods and applications of palladium nanoparticles: A review. *Front. Nanotechnol.* **2022**, *4*, 92. [[CrossRef](#)]
12. Lung, J.K.; Huang, J.C.; Tien, D.C.; Liao, C.Y.; Tseng, K.H.; Tsung, T.T.; Kao, W.S.; Tsai, T.H.; Jwo, C.S.; Lin, H.M.; et al. Preparation of gold nanoparticles by arc discharge in water. *J. Alloy. Compd.* **2007**, *434*, 655–658. [[CrossRef](#)]
13. Thakkar, K.N.; Mhatre, S.S.; Parikh, R.Y. Biological synthesis of metallic nanoparticles. *Nanomed. Nanotechnol. Biol. Med.* **2010**, *6*, 257–262. [[CrossRef](#)]
14. Varma, R.S. Greener approach to nanomaterials and their sustainable applications. *Curr. Opin. Chem. Eng.* **2012**, *1*, 123–128. [[CrossRef](#)]
15. Lazar, O.A.; Moise, C.C.; Nikolov, A.S.; Enache, L.B.; Mihai, G.V.; Enachescu, M. The Water-Based Synthesis of Platinum Nanoparticles Using KrF Excimer Laser Ablation. *Nanomaterials* **2022**, *12*, 348. [[CrossRef](#)]
16. Zhang, J.; Claverie, J.; Chaker, M.; Ma, D. Colloidal metal nanoparticles prepared by laser ablation and their applications. *ChemPhysChem* **2017**, *18*, 986–1006. [[CrossRef](#)]
17. Khashan, K.S.; Mahdi, F. Synthesis of ZnO:Mg nanocomposite by pulsed laser ablation in liquid. *Surf. Rev. Lett.* **2017**, *24*, 1750101. [[CrossRef](#)]
18. Khashan, K.S.; Abbas, S.F. Characterization of InN nanoparticles prepared by laser as photodetector. *Int. J. Mod. Phys. B* **2016**, *30*, 1650080. [[CrossRef](#)]
19. Khashan, K.S.; Hassan, A.I.; Addie, A.J. Characterization of CuO thin films deposition on porous silicon by spray pyrolysis. *Surf. Rev. Lett.* **2016**, *23*, 1650044. [[CrossRef](#)]
20. Khashan, K.S.; Abbas, S.F. Indium nitride nanoparticles prepared by laser ablation in liquid. *Int. J. Nanosci.* **2019**, *18*, 1850021. [[CrossRef](#)]
21. Orooji, Y.; Ghanbari Gol, H.; Jaleh, B.; Rashidian Vaziri, M.R.; Eslamipannah, M. Large optical nonlinearity of the activated carbon nanoparticles prepared by laser ablation. *Nanomaterials* **2021**, *11*, 737. [[CrossRef](#)]
22. Zhang, D.; Choi, W.; Jakobi, J.; Kalus, M.R.; Barcikowski, S.; Cho, S.H.; Sugioka, K. Spontaneous shape alteration and size separation of surfactant-free silver particles synthesized by laser ablation in acetone during long-period storage. *Nanomaterials* **2018**, *8*, 529. [[PubMed](#)]
23. Chichkov, B.N.; Momma, C.; Nolte, S.; Von Alvensleben, F.; Tünnermann, A. Femtosecond, picosecond and nanosecond laser ablation of solids. *Appl. Phys. A* **1996**, *63*, 109–115. [[CrossRef](#)]
24. Duque, J.S.; Madrigal, B.M.; Riascos, H.; Avila, Y.P. Colloidal metal oxide nanoparticles prepared by laser ablation technique and their antibacterial test. *Colloids Interfaces* **2019**, *3*, 25. [[CrossRef](#)]
25. Mostafa, A.M.; Mwafy, E.A. The effect of laser fluence for enhancing the antibacterial activity of NiO nanoparticles by pulsed laser ablation in liquid media. *Environ. Nanotechnol. Monit. Manag.* **2020**, *14*, 100382. [[CrossRef](#)]
26. Hadi, A.A.; Badr, B.A.; Mahdi, R.O.; Khashan, K.S. Rapid laser fabrication of Nickel oxide nanoparticles for UV detector. *Optik* **2020**, *219*, 165019.
27. Kebede, A.; Gholap, A.V.; Rai, A.K. Impact of laser energy on synthesis of iron oxide nanoparticles in liquid medium. *World J. Nano Sci. Eng.* **2011**, *1*, 89–92. [[CrossRef](#)]
28. Khashan, K.S.; Taha, J.M.; Abbas, S.F. Fabrication and Properties of InN NPs/Si as a photodetector. *Energy Procedia* **2017**, *119*, 656–661. [[CrossRef](#)]
29. Marzun, G.; Nakamura, J.; Zhang, X.; Barcikowski, S.; Wagener, P. Size control and supporting of palladium nanoparticles made by laser ablation in saline solution as a facile route to heterogeneous catalysts. *Appl. Surf. Sci.* **2015**, *348*, 75–84. [[CrossRef](#)]
30. Mendivil, M.I.; Krishnan, B.; Castillo, G.A.; Shaji, S. Synthesis and properties of palladium nanoparticles by pulsed laser ablation in liquid. *Appl. Surf. Sci.* **2015**, *348*, 45–53. [[CrossRef](#)]
31. Cristoforetti, G.; Pitzalis, E.; Spiniello, R.; Ishak, R.; Muniz-Miranda, M. Production of palladium nanoparticles by pulsed laser ablation in water and their characterization. *J. Phys. Chem. C* **2011**, *115*, 5073–5083. [[CrossRef](#)]
32. Khashan, K.S.; Ismail, R.A.; Mahdi, R.O. Synthesis of SiC nanoparticles by SHG 532 nm Nd:YAG laser ablation of silicon in ethanol. *Appl. Phys. A* **2018**, *124*, 443. [[CrossRef](#)]
33. Boutinguiza, M.; Meixus, M.; Del Val, J.; Riveiro, A.; Comesaña, R.; Lusquiños, F.; Pou, J. Synthesis and characterization of Pd nanoparticles by laser ablation in water using nanosecond laser. *Phys. Procedia* **2016**, *83*, 36–45. [[CrossRef](#)]
34. Jahangirian, H.; Haron, M.J.; Shah, M.H.; Abdollahi, Y.A.; Rezayi, M.A.; Vafaei, N.A. Well diffusion method for evaluation of antibacterial activity of copper phenyl fatty hydroxamate synthesized from canola and palm kernel oils. *Dig. J. Nanomater. Biostruct.* **2013**, *8*, 1263–1270.
35. Sarmah, M.; Neog, A.B.; Boruah, P.K.; Das, M.R.; Bharali, P.; Bora, U. Effect of substrates on catalytic activity of biogenic palladium nanoparticles in C–C cross-coupling reactions. *ACS Omega* **2019**, *4*, 3329–3340. [[CrossRef](#)] [[PubMed](#)]
36. Siddiqi, K.S.; Husen, A. Green synthesis, characterization and uses of palladium/platinum nanoparticles. *Nanoscale Res. Lett.* **2016**, *11*, 1–13. [[CrossRef](#)] [[PubMed](#)]
37. Fernández-Arias, M.; Vilas, A.M.; Boutinguiza, M.; Rodríguez, D.; Arias-González, F.; Pou-Álvarez, P.; Riveiro, A.; Gil, F.J.; Pou, J. Palladium Nanoparticles Synthesized by Laser Ablation in Liquids for Antimicrobial Applications. *Nanomaterials* **2022**, *12*, 2621. [[CrossRef](#)]

38. Nasrollahzadeh, M.; Sajadi, S.M.; Honarmand, E.; Maham, M. Preparation of palladium nanoparticles using *Euphorbia thymifolia* L. leaf extract and evaluation of catalytic activity in the ligand-free Stille and Hiyama cross-coupling reactions in water. *New J. Chem.* **2015**, *39*, 4745–4752. [[CrossRef](#)]
39. Xu, L.; Wu, X.C.; Zhu, J.J. Green preparation and catalytic application of Pd nanoparticles. *Nanotechnology* **2008**, *19*, 305603. [[CrossRef](#)]
40. Patel, K.; Kapoor, S.; Dave, D.P.; Mukherjee, T. Synthesis of Pt, Pd, Pt/Ag and Pd/Ag nanoparticles by microwave-polyol method. *J. Chem. Sci.* **2005**, *117*, 311–316. [[CrossRef](#)]
41. Šmejkal, P.; Pflieger, J.; Vlčková, B. Study of laser fragmentation process of silver nanoparticles in aqueous media. *Appl. Phys. A* **2008**, *93*, 973–976. [[CrossRef](#)]
42. Dittrich, S.; Barcikowski, S.; Bilal, G. Plasma and nanoparticle shielding during pulsed laser ablation in liquids cause ablation efficiency decrease. *Opto-Electron. Adv.* **2021**, *4*, 01200072. [[CrossRef](#)]
43. Kim, J.; Reddy, D.A.; Ma, R.; Kim, T.K. The influence of laser wavelength and fluence on palladium nanoparticles produced by pulsed laser ablation in deionized water. *Solid State Sci.* **2014**, *37*, 96–102. [[CrossRef](#)]
44. Desarkar, H.S.; Kumbhakar, P.; Mitra, A.K. Linear optical absorption and photoluminescence emission properties of gold nanoparticles prepared by laser ablation technique. *Appl. Phys. A* **2012**, *108*, 81–89. [[CrossRef](#)]
45. Al-Jumaili, A.; Alancherry, S.; Bazaka, K.; Jacob, M.V. Review on the antimicrobial properties of carbon nanostructures. *Materials* **2017**, *10*, 1066. [[CrossRef](#)]
46. Salazar, L.; Vallejo López, M.J.; Grijalva, M.; Castillo, L.; Maldonado, A. Biological effect of organically coated *Grias neuberthii* and *Persea americana* silver nanoparticles on HeLa and MCF-7 cancer cell lines. *J. Nanotechnol.* **2018**. [[CrossRef](#)]
47. Gopinath, K.; Gowri, S.; Arumugam, A. Phytosynthesis of silver nanoparticles using *Pterocarpus santalinus* leaf extract and their antibacterial properties. *J. Nanostruct. Chem.* **2013**, *3*, 68. [[CrossRef](#)]
48. Liu, S.; Lai, Y.; Zhao, X.; Li, R.; Huang, F.; Zheng, Z.; Ying, M. The influence of H₂O₂ on the antibacterial activity of ZnO. *Mater. Res. Express* **2019**, *6*, 0850c6. [[CrossRef](#)]

Disclaimer/Publisher's Note: The statements, opinions and data contained in all publications are solely those of the individual author(s) and contributor(s) and not of MDPI and/or the editor(s). MDPI and/or the editor(s) disclaim responsibility for any injury to people or property resulting from any ideas, methods, instructions or products referred to in the content.